Sensor-aided Camera Calibration for Three Dimensional Digital Image Correlation Measurements

Fabio Bottalico*[1], Nicholas A. Valente[1], Christopher Niezrecki[1], Kshitij Jerath[1], Yan Luo[2], and Alessandro Sabato[1]
[1] Department of Mechanical Engineering, University of Massachusetts Lowell, 1 University Avenue, Lowell, MA 01854, USA
[2] Department of Electrical and Computer Engineering, University of Massachusetts Lowell, 1 University Avenue, Lowell, MA 01854, USA
Fabio_Bottalico@student.uml.edu *(Corresponding author)

ABSTRACT

Stereovision systems can extract full-field three-dimensional (3D) displacements of structures by processing the images collected with two synchronized cameras. To obtain accurate measurements, the cameras must be calibrated to account for lens distortion (i.e., intrinsic parameters) and compute the cameras' relative position and orientation (i.e., extrinsic parameters). Traditionally, calibration is performed by taking photos of a calibration object (e.g., a checkerboard) with the two cameras. Because the calibration object must be similar in size to the targeted structure, measurements on large-scale structures are highly impractical. This research proposes a multi-sensor board with three inertial measurement units and a laser distance meter to compute the extrinsic parameters of a stereovision system and streamline the calibration procedure. In this paper, the performances of the proposed sensor-based calibration are compared with the accuracy of the traditional image-based calibration procedure. Laboratory experiments show that cameras calibrated with the multi-sensor board measure displacements with 95% accuracy compared to displacements obtained from cameras calibrated with the traditional procedure. The results of this study indicate that the sensor-based approach can increase the applicability of 3D digital image correlation measurements to large-scale structures while reducing the time and complexity of the calibration.

Keywords: Camera calibration, Digital image correlation, Stereophotogrammetry, Sensors, Large-area calibration.

1. INTRODUCTION

Traditional contact-based measurements for structural health monitoring (SHM) come with some drawbacks, the most important one being the inability to provide full-field measurements. On the contrary, computer vision (CV) and photogrammetry methods inherently overcome this limitation and are gaining popularity in the SHM community [1,2]. Among the available photogrammetry techniques, three-dimensional (3D) digital image correlation (DIC) has been increasingly used in the SHM community to extract shapes, displacements, and strain profiles from pictures acquired using synchronized stereo cameras [3, 4]. 3D-DIC has shown accuracy comparable to traditional contact-bases sensors when used to perform measurements in a plethora of engineering domains [5-9]and scales [10] with cameras both fixed and embedded on moving platforms [11,12].

3D-DIC works by identifying the 2D projection of a 3D point ***P*** onto the retinal planes of the cameras composing the stereovision system. The 3D location of point ***P*** is reconstructed by using triangulation, and then tracked in time across a set of synchronized pictures captured as the point moves with respect to the two cameras (see Figure 1a). However, triangulation is only possible if the cameras' internal parameters (i.e., intrinsic parameters), relative position and relative orientation (i.e., extrinsic parameters) are known beforehand. The process to obtain said parameters is called stereo calibration [13]. For a field of view (FOV) up to ~ 2 meters, calibration is traditionally performed by acquiring a set of synchronized pictures of calibration objects containing traceable optical targets whose positions are well-known (see Figure 1b). From those pictures, an algorithm called bundle adjustment computes the full set of camera intrinsic and extrinsic parameters [14]. However, once the cameras are calibrated, their relative position cannot be altered to prevent

measurement errors due to loss of calibration. As such, cameras are rigidly mounted to a stiff bar or fixed on stable tripods, which limits the applicability of 3D-DIC for SHM.

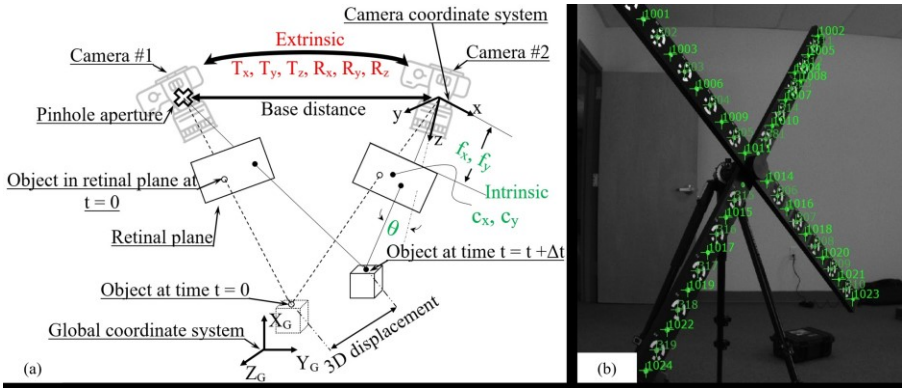

Figure 1: Overview of the principles behind 3D-DIC: a) representation of the physical meaning of intrinsic and extrinsic parameters, with an example of object tracking in 3D space and b) example of calibration cross (arm length: 1800 mm) used to calibrate stereovision systems, with coded optical targets highlighted in green.

To properly calibrate the cameras, the size of the targeted structure must be comparable with the size of the calibration object. This means that the calibration object must have approximately the same size of the FOV of the stereovision system. As the size of the FOV increases beyond ~2 meters, a different calibration procedure, known as large-area calibration, must be performed [9]. This procedure requires custom-made calibration objects, larger mounting bars to ensure the cameras are locked in position, and multiple hours of work due to the increased complexity. All those constraints limit the use of 3D-DIC for monitoring of large-scale structures.

For these reasons, multiple approaches are being developed as an alternative to traditional calibration methods. Due to the separability of a stereovision system's intrinsic and extrinsic parameters, researchers are currently looking for alternative ways to compute the extrinsic parameters. Some examples include using a single image of multiplanar [15] or cylinder-shaped [16] calibration objects, collecting multiple images of a scale bar [17], measuring the phase-shift of active targets [18,19], and relying on the detection of single feature points [20]. However, those procedures are still affected by the drawbacks of a traditional image-based calibration, such as the loss of calibration after the cameras are moved relatively to each other.

To reduce the complexity and increase the flexibility of calibration, the use of sensors has been proposed. However, these approaches still require images of a calibration object, as the sensor data are only used to complement the image data [21]. Recently, a new approach to compute the extrinsic parameters using data coming exclusively from sensors, without using images of a calibration object, has been proposed [22 -25]. This paper describes the validation experiments performed to characterize the accuracy of a newly proposed multi-sensor system to extract the extrinsic calibration parameters needed to perform 3D-DIC measurements. In this research, 3D-DIC measurements obtained with cameras calibrated with the traditional image-based approach are compared to measurements performed with cameras calibrated using the proposed sensor-based approach. An extensive laboratory campaign on medium-sized FOVs (i.e., 3 – 5 m) shows how the sensor-based method yield results that are comparable to the traditional approach with an accuracy ~95%.

2. PROPOSED CALIBRATION METHOD AND MATHEMATICAL FRAMEWORK

A schematic of the proposed multi-sensor board is shown in Figure 2. The schematic shows the type of data acquired by each sensor and how the data is transported to Master Station for processing. Based off the schematic in Figure 2, a prototype of the multi-sensor board was built. The prototype used in this research to measure the extrinsic parameters of the stereovision system consists of two Basler puA1600-60uc cameras[26], fitted with 12 mm lenses, three LPMS-IG1 inertial measurement units (IMUs) manufactured by LP Research[27], one M88B laser module manufactured by JRT Measure[28], and

two Raspberry Pi 4. The two boards of the prototype are shown in Figure 3, while a characterization of the noise floor of the multi-sensor board is shown in previous papers from the authors [24,25].

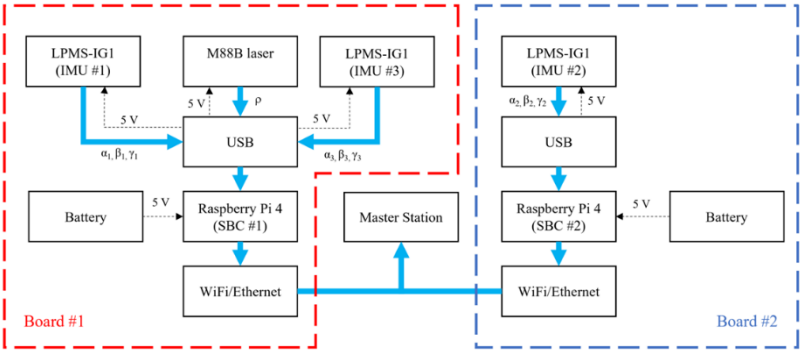

Figure 2. Schematic of the multi-sensor system's prototype used in this research to measure the extrinsic parameters of a stereovision system.

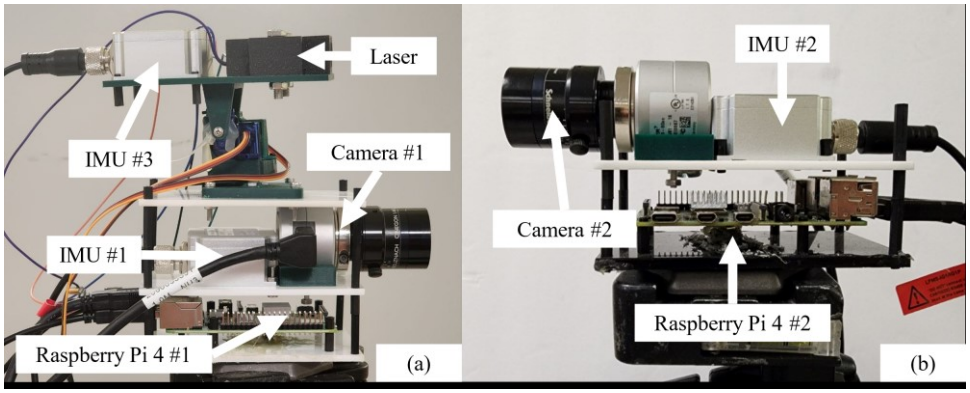

Figure 3: Prototype of the multi-sensor system, with indication of the components: a) view of Board #1 and b) view of Board #2.

In the proposed method, the IMUs and the laser module are used to estimate the cameras' extrinsic parameters through their rotation matrices $\boldsymbol{R_i}$ and translation vector $\boldsymbol{T}$. IMU #1 and IMU #2 are connected to the cameras and used to measure the roll α_i, pitch β_i, and yaw γ_i angles and compute the i-th camera $\boldsymbol{R_i}$ using Equation (1):

$$\boldsymbol{R_{W,i}} = \boldsymbol{R_z}(\gamma_i)\,\boldsymbol{R_y}(\beta_i)\,\boldsymbol{R_x}(\alpha_i) = \begin{bmatrix} cos(\gamma_i) & -sin(\gamma_i) & 0 \\ sin(\gamma_i) & cos(\gamma_i) & 0 \\ 0 & 0 & 1 \end{bmatrix} \begin{bmatrix} cos(\beta_i) & 0 & sin(\beta_i) \\ 0 & 1 & 0 \\ -sin(\beta_i) & 0 & cos(\beta_i) \end{bmatrix} \begin{bmatrix} 1 & 0 & 0 \\ 0 & cos(\alpha_i) & -sin(\alpha_i) \\ 0 & sin(\alpha_i) & cos(\alpha_i) \end{bmatrix} \quad (1)$$

where the subscript i identifies the camera's number (i.e., 1 or 2 in the proposed approach). The IMU #3 and the laser are rigidly mounted together onto a pan-tilt mechanism connected to Camera #1. Because all three IMUs measure angles relative to the user-defined global frame of reference W, the translation vector $\boldsymbol{T_W}$ is computed using the following equation:

$$\boldsymbol{T_W} = \left(\prod_n \boldsymbol{H_n^{n-1}}\right) * \begin{bmatrix} 0 \\ 0 \\ \rho \\ 1 \end{bmatrix} \quad (2)$$

where ρ is the relative distance between the cameras, measured by the laser, and $\boldsymbol{H_n^{n-1}}$ is the homogeneous transformation that uses the Denavit-Hartenberg (DH) parameters[29] to estimate the position of the laser sensor with respect to the optical

center of Camera #1. Given that the laser sensor is mounted on a pan-tilt mechanism, the lengths and orientations of the links composing the pan-tilt mechanism constitute the DH parameters. As a result, the vector $\boldsymbol{T_W}$ computed with Equation (2) represents the translation vector between the optical center of Camera #1 and the optical center of Camera #2 expressed in the global frame of reference *W*. Once $\boldsymbol{R_{W,1}}$, $\boldsymbol{R_{W,2}}$, and $\boldsymbol{T_W}$ are obtained, they must be expressed into Camera #1's frame of reference to be used as extrinsic parameters for the stereovision system. This transformation is achieved using Equation (3):

$$\begin{cases} \boldsymbol{R_{12}} = \boldsymbol{R_{W,1}^T R_{W,2}} \\ \boldsymbol{T_{12}} = \boldsymbol{R_{W,1}^T T_W} \end{cases} \tag{3}$$

where $\boldsymbol{R_{12}}$ is the relative rotation matrix between Camera #2 and Camera #1 expressed in the frame of reference of Camera #1 while $\boldsymbol{T_{12}}$ is the translation vector between Camera #1 and Camera #2 expressed in the frame of reference of Camera #1.

Once all the terms of Equation (3) are computed, the full set of extrinsic parameters of the stereo camera system is determined and can be used to perform a 3D-DIC analysis.

3. EXPERIMENTAL SETUP

Two experiments were conducted to validate the accuracy of the proposed calibration method. In both tests, the cameras were calibrated using both the image-based and the sensor-based procedures. For the traditional calibration, multiple stereo images of a checkerboard calibration object were collected and used to extract the intrinsic and the extrinsic parameters of the stereovision system in the configuration used during the tests. For the sensor-based method, the intrinsic parameters were calibrated by taking pictures of a small checkerboard calibration object placed in front of the cameras focused on the targeted object, while the extrinsic parameters were extracted using the procedure described in Section 2 using the data from the IMUs and the laser sensor. The resulting calibration files (i.e., one from the traditional image-based method and one from the proposed sensor-based approach) were then used to process the stereo images collected during the two experiments and extract the 3D displacement of the objects being tested.

In Test #1, a laboratory-scale wind turbine blade with length equal to 2.3 m was quasi-statically deformed in the out-of-plane direction and the two cameras were used to extract the Z-displacement of the structure. The cameras were placed to have a working distance of 3 m from the blade, a camera separation distance of 1.4 m, and a camera separation angle of 26.2°, which resulted in a calibrated volume of ~ 3 x 1.5 x 3 m.

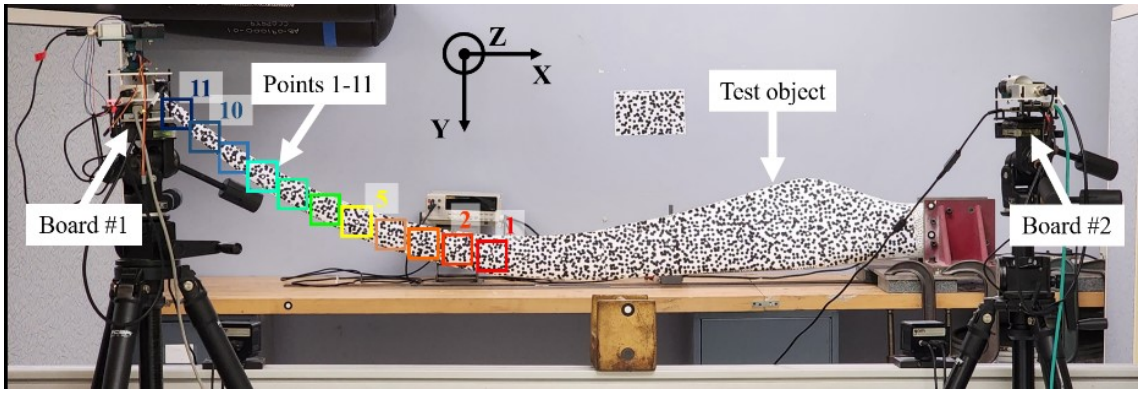

Figure 4: Overview of the experimental setup used to measure the out-of-plane displacement of a laboratory-scale wind turbine blade.

As shown in Figure 4, that represents an overview of the experimental setup used during Test #1, the surface of the blade was painted with a stochastic speckle pattern to allow the use of 3D-DIC. In addition, eleven optical targets were attached on the centerline of the blade to allow extracting the out-of-plane displacement and compare the measurements obtained with the cameras calibrated with traditional and sensor-based procedures at specific locations. In particular, Point 1 is the optical target closer to the root of the blade, while Point 11 is the one towards the tip of the blade. Before starting the tests, five images of the blade at rest (i.e., without any force applied to it) were collected and used to evaluate the noise floor

(NF) of the measurement. Subsequently, the blade's tip was displaced by finite increments in the out-of-plane direction and, for each incremental displacement, five stereo images were captured. During Test #1, a total of eleven displacements were applied to the blade (i.e., five loading and five unloading).

In Test #2, a 0.8 x 0.6 m planar object with an applied stochastic pattern was moved in a 3D space with dimension of 4.0 x 3.0 x 3.5 m. Because Test #2 aimed at assessing the performance of the sensor-based calibration for larger FOVs, the cameras were placed to have a working distance of 6.5 m from the planar object, a cameras' separation distance of 4.4 m, and a cameras' separation angle of 38°. An overview of the setup is shown in Figure 5.

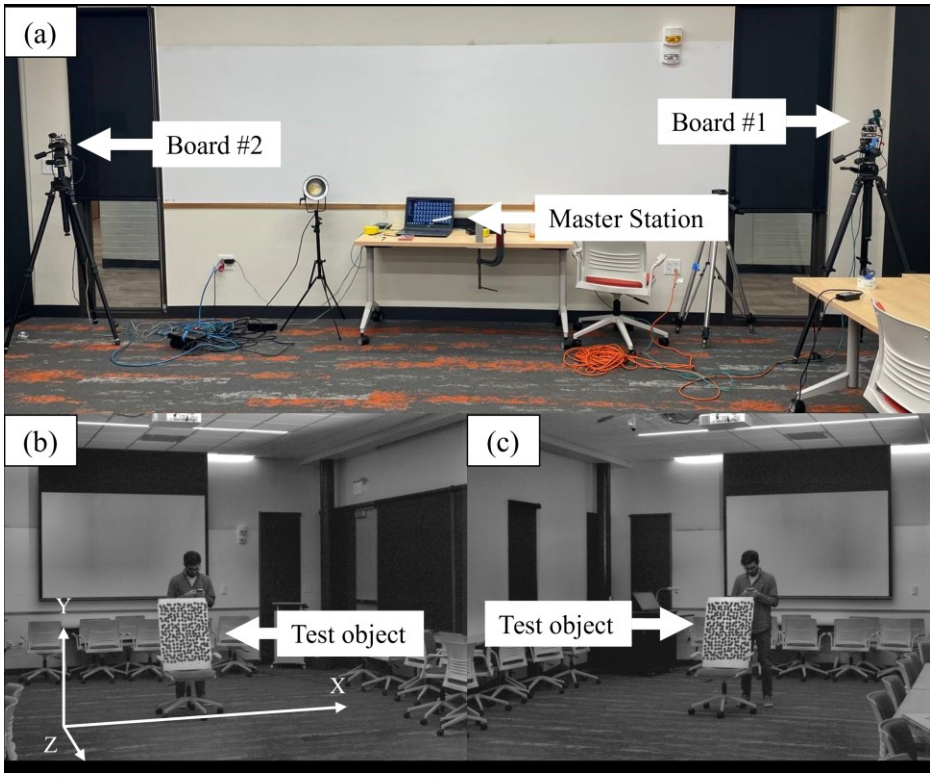

Figure 5: Overview of the experimental setup used to measure the 3D displacements of the planar object: a) cameras and master station used to trigger the multi-sensor boards, b) sample image of the planar object (seen from the left camera's perspective) with indication of the frame of reference used for 3D-DIC, and c) sample image of the planar object (seen from the right camera's perspective).

For Test #2, the same testing procedure used for Test #1 was adopted. Once the cameras were calibrated, five initial stereo images of the planar object at full rest were captured to estimate the NF of the 3D-DIC measurements. Then, the planar object was displaced by applying an oscillatory motion in the Y-direction defined in Figure 5b, while being also rigidly moved in the X-direction and images were acquired with the two synchronized cameras.

4. ANALYSIS OF THE RESULTS

For both tests, the open-source software Digital Image Correlation Engine (DICe) [30] was used to process the collected images and extract the displacement of the test objects when the stereovision system is calibrated using **i)** the traditional image-based method and **ii)** the proposed sensor-based calibration based on the measurement performed with the multi-sensor board. This section summarizes the results of the two tests performed.

4.1 Results of tests performed on lab-scale wind turbine blade

Figure 6 shows the NF of the two measurements when the only difference in the procedure is the type of calibration used.

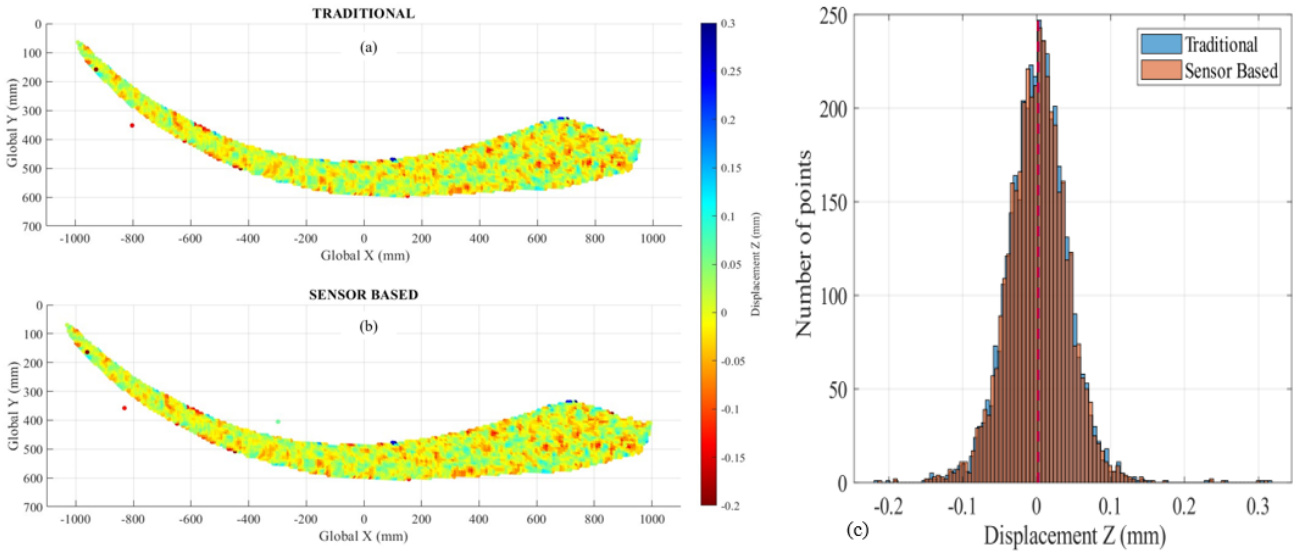

Figure 6: Comparison of the measurements obtained when the calibration is performed using the traditional image-based method and the multi-sensor board for Test#1: a) out-of-plane (i.e., Z-displacement) noise floor computed with traditional calibration, b) out-of-plane (i.e., Z-displacement) noise floor computed with sensor-based calibration, and c) distribution of the noise floor computed using the two methods.

It can be seen from Figure 6 that the NF of the measurement obtained when the cameras are calibrated using the proposed sensor-based method (see Figure 6b) visually matches the NF of the measurement that is obtained when the cameras are calibrated using a traditional image-based method (see Figure 6a). Additionally, the NF distributions follow a Gaussian distribution and qualitatively show a significant overlap. From a quantitative standpoint, it is possible to assess the correlation between the two NFs by computing the Kullback-Leibler (K-L) Divergence [31] of the two distributions (see Figure 6c). For the case-study discussed in this paper, the K-L divergence between the NFs of the two measurements is 3.3, indicating extremely high similarity.

When the results of the measurements done to quantify the out-of-plane displacement applied to the blade are processed, the results shown in Figure 7 are obtained. When discrepancies between the results obtained using the two different calibrations are analyzed in Figure 7a, it is observed that the largest difference is always smaller than 0.14 mm at the point of maximum displacement (i.e., Point 11 – tip of the blade). Figure 7b shows that the relative difference between the two sets of data is consistently below 5%, with relative errors smaller than 1% for the point of maximum displacement.

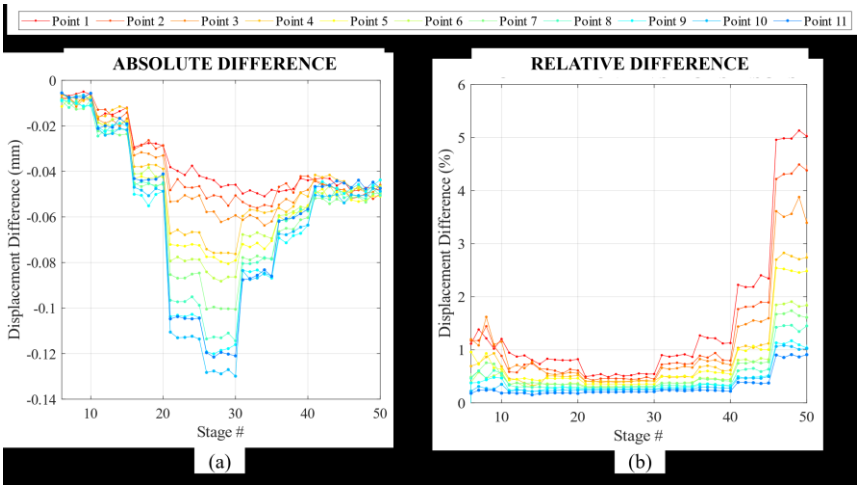

Figure 7: Difference between the out-of-plane displacements computed with the traditional calibration and the proposed sensor-based calibration: a) absolute difference and b relative difference.

These results prove the accuracy of the proposed sensor-based approach when data retrieved using the prototype shown in Figure 3 is used for 3D-DIC measurement on medium-sized objects.

4.2 Results of tests performed on planar object

For Test #2, the results of the in-plane and out-of-plane NFs obtained from cameras calibrated using the two methods are shown in Figure 8. Similarly to the results of Test #1, the NF of Test #2 shows good agreement between the measurements obtained with the traditional calibration and the proposed sensor-based calibration (see Figure 9). As can be observed from the figure, the NF distributions have similar trend and comparable overlap with those shown in Figure 6c. When the similarity between the distributions obtained from the traditional and sensor-based calibrations are quantified, the K-L divergences have values equal to 2.97, 1.77 and 7.06 for the NF in the X, Y and Z directions, respectively.

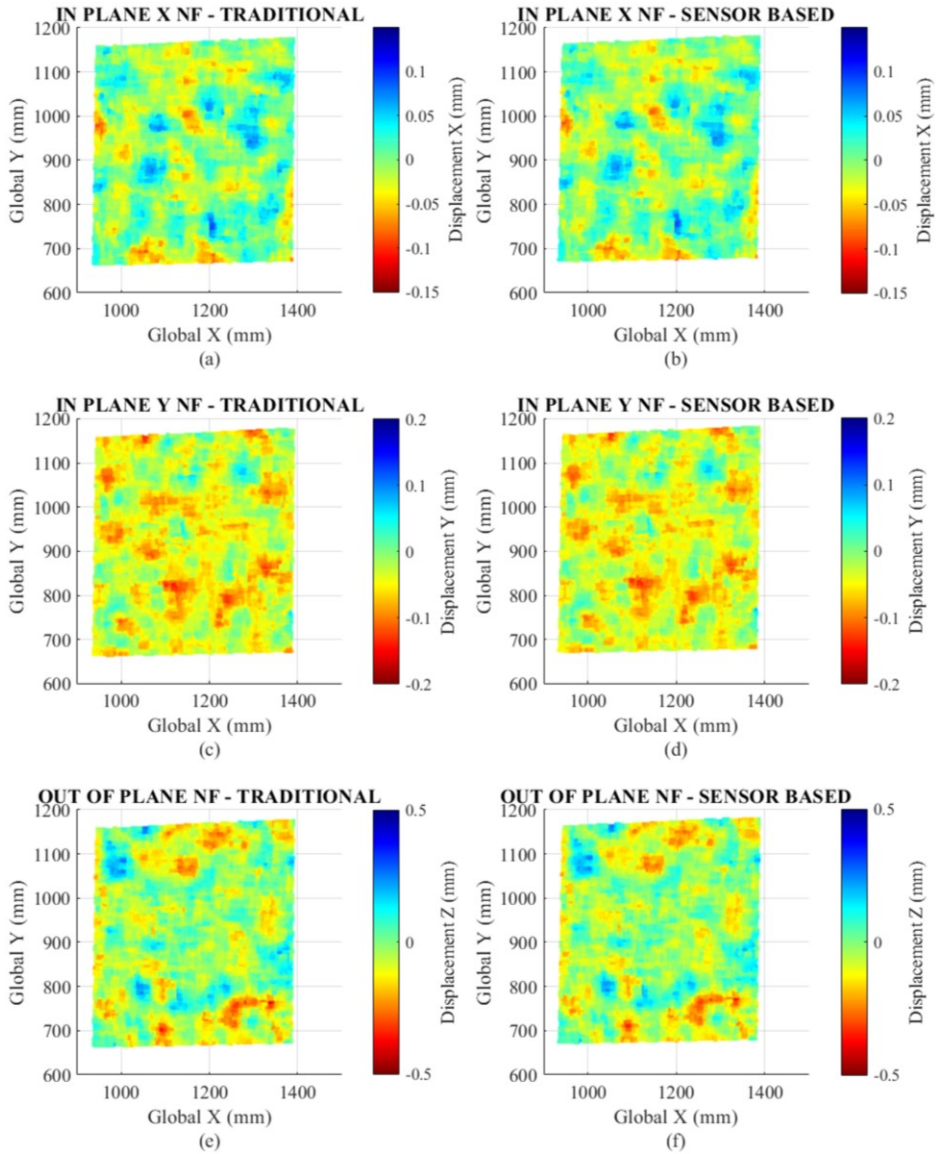

Figure 8: Noise floors of the measurements performed on the planar object, computed with the traditional image-based calibration and the proposed sensor-based calibration: a) in-plane X displacement from traditional calibration, b) in-plane X displacement from sensor-based calibration, c) in-plane Y displacement from traditional calibration, d) in-plane Y displacement from sensor-based calibration, e) out-of-plane Z displacement from traditional calibration, and f) out-of-plane Z displacement from sensor-based calibration.

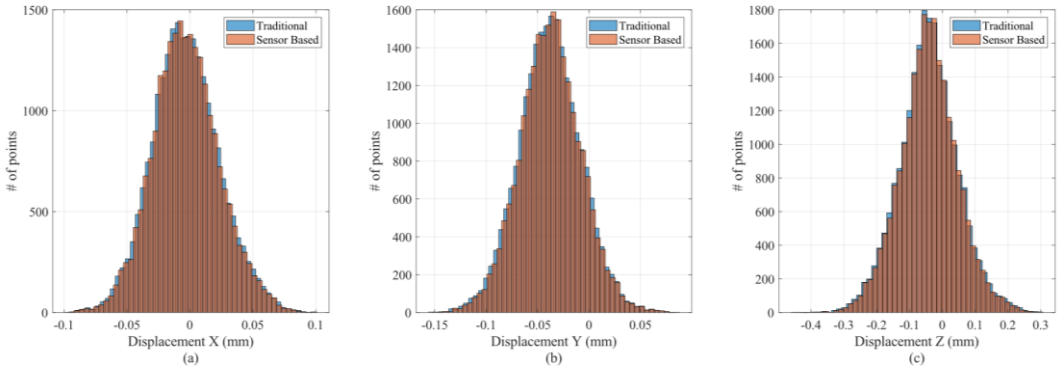

Figure 9: Histograms of the noise floors for the measurements performed for Test #2 for: a) X-direction displacement, b) Y-direction displacement, and c) Z-direction displacement.

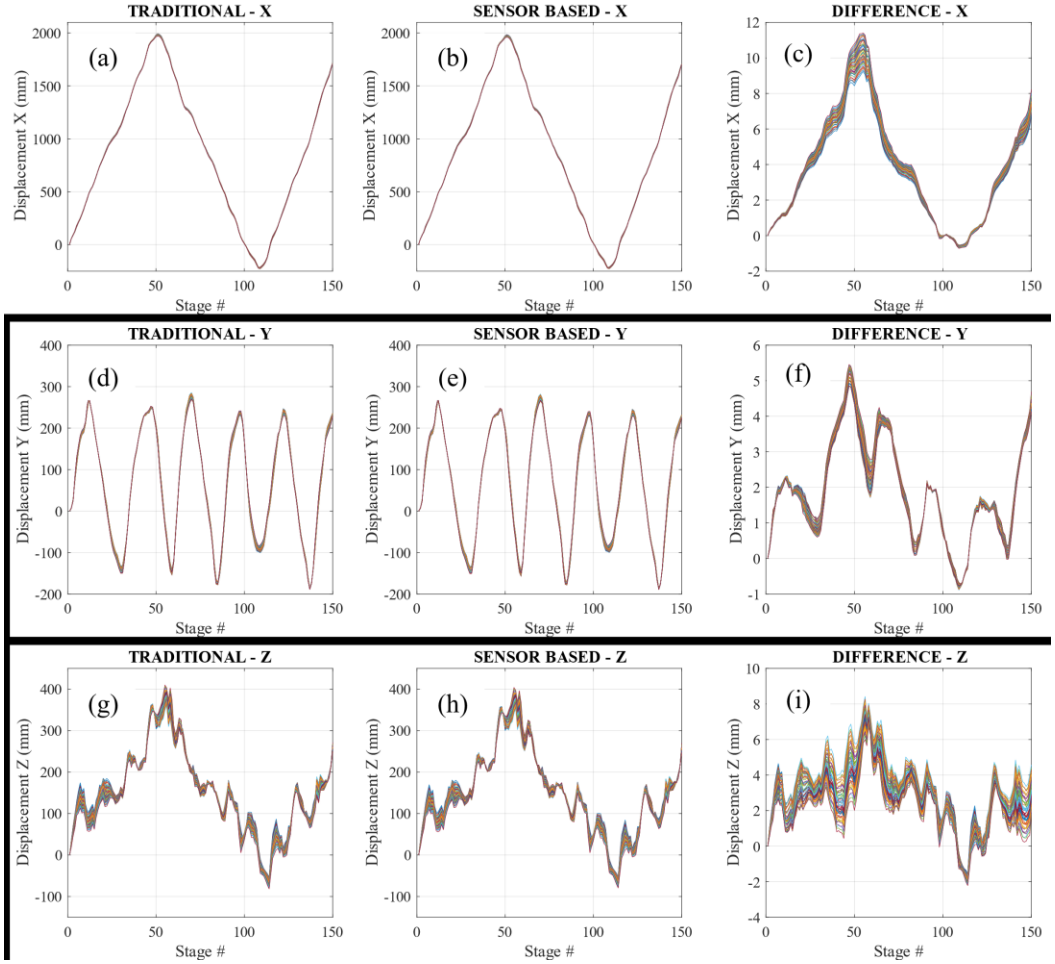

Figure 10: 3D trajectories of the planar object's 49 reference points; a) in-plane X displacement from traditional calibration, b) in-plane X displacement from sensor-based calibration, c) difference between the in-plane X displacement computed with both traditional and sensor-based calibration, d) in-plane Y displacement from traditional calibration, e) in-plane Y displacement from sensor-based calibration, f) difference between the in-plane Y displacement computed with both traditional and sensor-based calibration, g) out-of-plane Z displacement from traditional calibration, h) out-of-plane Z displacement from sensor-based calibration, and i) difference between the out-of-plane Z displacement computed with both traditional and sensor-based calibration.

Before processing the images, it should be pointed out that 49 reference points in a 7x7 grid were identified on the surface of the planar object and tracked through the images collected during Test #2 to quantify the displacement of the object of interest. The trajectory of the planar object over time measured from the images processed using the two different calibrations is shown in Figure 10. In particular, the first two columns of Figure 10 show the X, Y, and Z-direction displacements obtained with the traditional calibration (see Figure 10a, Figure 10d, and Figure 10g) and the sensor-based calibration (see Figure 10b, Figure 10e, and Figure 10h). The last column in Figure 10 shows the difference between the two datasets. From the analysis of those results it is possible to observe that the maximum difference in the out-of-plane direction (i.e., ~8 mm) is on the same order of magnitude the maximum difference in the in-plane direction (~12 mm) despite the in-plane displacements being 5 times larger. The percentage difference between the methods amount to ~ 0.65% in the in-plane direction and ~2% in the out-of-plane direction. Additionally, it can be observed that all 49 reference points appear to move by the same amount along the same trajectory computed with either calibration, with discrepancies in the magnitudes of the motion that are almost unnoticeable for the in-plane displacements (see Figure 10a, Figure 10b, Figure 10d, and Figure 10e) and that start being noticeable for the out-of-plane displacements (see Figure 10g and Figure 10h). However, even though the difference between the two calibration methods is larger in magnitude at larger displacements, the relative difference in percentage is significantly small, thus confirming that the sensor-based calibration produces 3D-DIC measurements in very good agreement with those produced by a traditional calibration.

5. CONCLUSIONS

This research proposes a novel method to measure the extrinsic parameters of a stereovision system for 3D-DIC. By measuring the orientation of two synchronized cameras using three (IMUs, their relative distance using a laser, the proposed method computes a full set of extrinsic parameters to calibrate the stereovision system. Laboratory tests were performed to characterize the accuracy and viability of the proposed method. When measuring the out-of-plane deformations imparted to a lab-scale wind turbine blade, the proposed approach is able to provide extrinsic parameters such that the measurement obtained with the proposed calibration and measurements obtained with a traditional image-based calibration differ by less than 5% overall, and less than 1% at the point of maximum displacement. Similarly, when used to quantify the 3D displacements of a planar object in a large-area experiment (i.e., 4 x 3 x 3.5 m), the measurements obtained with the proposed calibration differ from the measurements obtained with a traditional image-based calibration by less than 1% in the in-plane directions and ~2% in the out-of-plane direction. This research validates how the proposed method is a viable alternative to image-based calibration methods and can extend the usability of 3D-DIC to larger fields of view, thus opening the possibility to use this technique for long-term monitoring of large-scale structures.

ACKNOWLEDGEMENT

This work was supported by the U.S. National Science Foundation (NSF) under award number 2018992, "*MRI: Development of a calibration system for stereophotogrammetry to enable large-scale measurement and monitoring*." The contents are those of the authors and do not necessarily represent the official views of the funding agency.

REFERENCES

[1] D. Feng, and M. Q. Feng, "Computer vision for SHM of civil infrastructure: From dynamic response measurement to damage detection – A review," Engineering Structures, 156, 105-117 (2018).

[2] A. Sabato, S. Dabetwar, N. N. Kulkarni, *et al.*, "Non-contact sensing techniques for AI-aided structural health monitoring: a systematic review," IEEE Sensors Journal, 1-1 (2023).

[3] P. F. Luo, Y. J. Chao, M. A. Sutton *et al.*, "Accurate measurement of three-dimensional deformations in deformable and rigid bodies using computer vision," Experimental Mechanics, 33(2), 123-132 (1993).

[4] M. A. Sutton, J.-J. Orteu, and H. W. Schreier, "Two-Dimensional and Three-Dimensional Computer Vision", Image Correlation for Shape, Motion and Deformation Measurements: Basic Concepts,Theory and Applications, pp. 1-16 (2009).

[5] A. Sabato, and C. Niezrecki, "Feasibility of Digital Image Correlation for railroad tie inspection and ballast support assessment," Measurement, 103, 93-105 (2017).

[6] M. Shafiei Dizaji, M. Alipour, and D. K. Harris, “Leveraging Full-Field Measurement from 3D Digital Image Correlation for Structural Identification,” Experimental Mechanics, 58, 1049-1066 (2018).
[7] D. Gorjup, J. Slavič, and M. Boltežar, “Frequency domain triangulation for full-field 3D operating-deflection-shape identification,” Mechanical Systems and Signal Processing, 133, (2019).
[8] L. Ngeljaratan, and M. A. Moustafa, “Structural health monitoring and seismic response assessment of bridge structures using target-tracking digital image correlation,” Engineering Structures, 213, 110551 (2020).
[9] P. Poozesh, A. Sabato, A. Sarrafi *et al.*, “Multicamera measurement system to evaluate the dynamic response of utility-scale wind turbine blades,” Wind Energy, 23(7), 1619-1639 (2020).
[10] B. A. Lingga, D. B. Apel, M. Sepehri *et al.*, “Assessment of digital image correlation method in determining large scale cemented rockfill strains,” International Journal of Mining Science and Technology, 29(5), 771-776 (2019).
[11] D. Reagan, A. Sabato, and C. Niezrecki, “Feasibility of using digital image correlation for unmanned aerial vehicle structural health monitoring of bridges,” Structural Health Monitoring, 17(5), 1056-1072 (2018).
[12] M. Kalaitzakis, N. Vitzilaios, D. C. Rizos *et al.*, “Drone-Based StereoDIC: System Development, Experimental Validation and Infrastructure Application,” Experimental Mechanics, 61(6), 981-996 (2021).
[13] Z. Zhang, “Camera Parameters (Intrinsic, Extrinsic)”, Computer Vision: A Reference Guide, pp. 81-85(2014).
[14] B. Triggs, P. F. McLauchlan, R. I. Hartley *et al.*, "Bundle Adjustment — A Modern Synthesis," Vision Algorithms: Theory and Practice, pp. 298-372 (2000).
[15] J. Zhang, J. Zhu, H. Deng *et al.*, “Multi-camera calibration method based on a multi-plane stereo target,” Applied Optics, 58(34), 9353-9359 (2019).
[16] D. Solav, K. M. Moerman, A. M. Jaeger *et al.*, “MultiDIC: An open-source toolbox for multi-view 3D digital image correlation,” IEEE Access, 6, 30520-30535 (2018).
[17] P. Sun, N.-G. Lu, M.-L. Dong *et al.*, “Simultaneous All-Parameters Calibration and Assessment of a Stereo Camera Pair Using a Scale Bar,” Sensors, 18(11), 3964 (2018).
[18] B. Chen, K. Genovese, and B. Pan, “Calibrating large-FOV stereo digital image correlation system using phase targets and epipolar geometry,” Optics and Lasers in Engineering, 150, 106854 (2022).
[19] K. Genovese, Y. Chi, and B. Pan, “Stereo-camera calibration for large-scale DIC measurements with active phase targets and planar mirrors,” Optics Express, 27(6), 9040-9053 (2019).
[20] Y. Wang, X. Wang, Z. Wan *et al.*, “A Method for Extrinsic Parameter Calibration of Rotating Binocular Stereo Vision Using a Single Feature Point,” Sensors, 18(11), 3666 (2018).
[21] W. Feng, Z. Su, Y. Han *et al.*, “Inertial measurement unit aided extrinsic parameters calibration for stereo vision systems,” Optics and Lasers in Engineering, 134, 106252 (2020).
[22] A. Sabato, and C. Niezrecki, “Development of an IMU-radar sensor board for three-dimensional digital image correlation camera triangulation”, Proc. SPIE 10972, SS (2019).
[23] A. Sabato, N. A. Valente, and C. Niezrecki, “Development of a Camera Localization System for Three-Dimensional Digital Image Correlation Camera Triangulation,” IEEE Sensors Journal, 20(19), 11518-11526 (2020).
[24] F. Bottalico, N. A. Valente, S. Dabetwar, *et al.*, “A sensor-based calibration system for three-dimensional digital image correlation”, Proc. SPIE 12048, SS (2022).
[25] F. Bottalico, C. Niezrecki, K. Jerath, *et al.*, “Sensor-Based Calibration of Camera’s Extrinsic Parameters for Stereophotogrammetry”, IEEE Sensors Journal, 1-1 (2023)
[26] “puA1600-60uc - Basler pulse” <https://www.baslerweb.com/en/products/cameras/area-scan-cameras/pulse/pua1600-60uc/ > (Feb. 11th 2023).
[27] “LPMS-IG1 Series: High Precision 9-Axis Inertial Measurement Unit (IMU) / AHRS with USB / CAN / RS232 / RS485 Connectivity and Optional GPS Receiver.” <https://lp-research.com/9-axis-imu-with-gps-receiver-series/> (Feb. 11th, 2023).
[28] “40m Professional Width Measuring Sensor.” <https://www.jrt-measure.com/long-range-distance-sensor/57660459.html> (Feb. 11th 2023).
[29] P.I. Corke, “A simple and systematic approach to assigning Denavit-Hartenberg parameters”. IEEE Transaction on Robotics, 23(3), 590-594 (2007).
[30] D.Z. Turner, “Digital Image Correlation Engine (DICe) Reference Manual” Sandia Report SAND2015-10606 O (2015). https://dicengine.github.io/dice/
[31] J.M. Joyce, “Kullback-Leibler Divergence”, International Encyclopaedia of Statistical Science, pp 720-722 (2011).